remote sensing

MDPI

Article

Subsidence of a Coal Ash Landfill in a Power Plant Observed by Applying PSInSAR to Sentinel-1 SAR Data

Youngnam Shin and Hoonyol Lee *

Department of Geophysics, Kangwon National University, Chuncheon 24341, Republic of Korea; shinyn1997@kangwon.ac.kr

* Correspondence: hoonyol@kangwon.ac.kr; Tel.: +82-33-250-8587

Abstract: We analyzed ground subsidence at the coal ash disposal sites of Stanton Energy Center, a power plant located in Orlando, Florida, USA, by applying 157 Sentinel-1 SAR images obtained between May 2017 and December 2022 in ascending orbit to the PSInSAR technique. A LiDAR DEM with 1 m posting was used for the DInSAR and StaMPS processing for PSInSAR. The results showed significant ground subsidence on the area where solar panels were installed on top of the coal ash landfill. The coal ash landfill was divided into three sites (A, B, and C) according to the landfill sequence. The spatially averaged PSInSAR showed subsidence rates of 7.3 mm/year, 6.2 mm/year, and 8.8 mm/year in sites A, B, and C, respectively. In particular, relatively newly deposited sites A and B showed a decreasing trend in subsidence rate with higher quadratic components in regression function, indicating a stabilization of the subsidence. On the other hand, the oldest site C exhibited the highest (and a relatively constant) subsidence rate, suggesting that the settlement occurred earlier and is now at a constant rate. It is also suspected that new dumping activity near C might have caused a higher subsidence rate than in sites A and B. No subsidence occurred at other solar panel installations on the ground outside the landfill, suggesting that the subsidence was caused by the gravitational compaction of the landfill materials rather than by the instability of the solar facilities. Comparison of PSInSAR results with lower resolution DEMs, such as SRTM and Copernicus DEM, showed range errors of the PS positions proportional to the height deviation from LiDAR DEM, highlighting the importance of accurate DEMs for the time-series analysis of SAR data.

Keywords: PSInSAR; landfill; subsidence; Sentinel-1; DEM

Citation: Shin, Y.; Lee, H. Subsidence of a Coal Ash Landfill in a Power Plant Observed by Applying PSInSAR to Sentinel-1 SAR Data. *Remote Sens.* **2023**, *15*, 4127. https://doi.org/10.3390/rs15174127

Academic Editors: Damien Dhont and Marine Larrey

Received: 27 July 2023
Revised: 20 August 2023
Accepted: 21 August 2023
Published: 23 August 2023

1. Introduction

Coal-fired power generation contributed approximately 26.8% of global energy production as of 2019 [1]. This method involves burning coal in thermal power plants to generate both electricity and thermal energy, resulting in the production of coal ash, also known as coal combustion residuals (CCRs), which is considered industrial waste. Around 53% of coal ash was recycled as of 2010 [2], primarily for purposes such as creating construction materials such as cement replacements, ceramics, and road construction materials [3–5]. The remaining portion was either disposed of through reclamation or accumulation in dumping sites.

However, coal ash poses significant environmental hazards, leading to water and soil pollution, as well as to adverse effects on human health, including increased disease incidence and mortality [6,7]. Therefore, the proper management and monitoring of coal ash disposal are of utmost importance. The likelihood of slope collapse in coal ash landfills is influenced by several factors, including inadequate ground compaction, lack of a secure leachate filling facility, and the risk of landfill gas sedimentation and waste layer compression [8]. The reuse of such landfills for purposes such as parks and golf courses can further increase the potential for slope instability.

In the past, there have been instances of coal ash leakage due to the collapse of storage facilities, leading to environmental pollution in locations such as the Tennessee River [9–11] and the Dan River [12–15]. These incidents highlight the inherent risks associated with storage facilities, including vulnerability to natural disasters and insufficient facility management. Moreover, the process of restoring contaminated areas after such leaks requires considerable time and effort. Preventing such incidents and addressing environmental pollution require prioritizing the safety of coal ash storage facilities and establishing continuous monitoring practices. However, obtaining comprehensive in situ data for monitoring poses challenges due to various natural factors and limitations related to economics, spatial coverage, and time constraints. Nonetheless, it is crucial to find innovative solutions to overcome these obstacles to ensure effective environmental protection and safety measures for coal ash storage facilities.

Remote sensing offers numerous advantages for monitoring, as it eliminates spatial constraints by utilizing image data according to specific user requirements. Compared to on-site equipment measurements, remote sensing is both cost-effective and feasible for periodic observations. One such technique, synthetic aperture radar (SAR) remote sensing, allows image acquisition irrespective of weather conditions or time of day [16].

The interferometric SAR (InSAR) technique, utilizing pairs of SAR images, enables the measurement of phase information related to earth surface elevation and displacement [17]. Additionally, the differential interferometric SAR (DInSAR) technique, which compensates for elevation-related phase contributions, proves highly effective in detecting subtle ground subsidence with exceptional precision at the scale of centimeters [18].

A recently developed method, persistent scatterer interferometric SAR (PSInSAR), builds upon conventional radar interferometry. This technique involves acquiring multiple DInSAR images in a particular area, leveraging persistent scatterers (PSs) such as dense urban structures, transmission towers, and rocks. PSInSAR yields statistically significant and precise long-term displacement measurements, even at sub-millimeter accuracy [19,20]. By utilizing these advanced remote sensing methods, it becomes possible to closely monitor and analyze surface changes and movements with remarkable detail and reliability.

The PSInSAR technique, known for its capability to analyze surface deformation, has found widespread applications in diverse fields, encompassing natural disasters such as earthquakes, volcanoes, and landslides, as well as human-induced activities such as quarries, abandoned mining sites, and artificial structures [21–26]. Surprisingly, no studies have been reported on ground subsidence in coal ash landfills utilizing the PSInSAR technique. The absence of such studies can be attributed mainly to the scarcity of PS in the surface of coal ash landfills, which limits the application of this method for monitoring subsidence in these specific areas.

In this research, our primary objective is to observe and analyze ground subsidence in a coal ash landfill located in Orlando, Florida, USA. To achieve this, we will utilize Sentinel-1 SAR images and the PSInSAR technique, which offers precise and comprehensive subsidence data. Fortunately, the presence of a solar power facility on the landfill site provides an abundance of PSs, which are crucial for our analysis. We also plan to investigate ground subsidence on a nearby flat area where a solar power facility was installed around the same period. By comparing the subsidence patterns in this area with the ones observed in the coal ash landfill, we aim to discern whether the subsidence in the landfill is due to structural issues in the solar power facility or related to the deposition of materials beneath the landfill.

Our study period spans from May 2017, when the solar panels' installation was completed, to December 2022. During this time, we will analyze the subsidence rate and patterns in the solar power facility area. For the coal ash landfill, we will utilize past digital elevation model (DEM) data and Google Earth images to understand the historical terrain changes. Additionally, we intend to investigate the relationship between the timing of waste disposal in the landfill and the patterns of ground subsidence using the PSInSAR technique. Furthermore, we will analyze the phenomenon of PS position shifting in areas

such as the landfill, where localized elevation changes are evident. Such shifts can occur due to errors in the DEM used during the processing of the PSInSAR data. Overall, this study aims to provide valuable insights into the factors influencing ground subsidence in the coal ash landfill area and the adjacent solar power facility, aiding in better understanding and management of potential subsidence risks.

2. Materials and Methods

2.1. Study Area

The study area under consideration is the Stanton Energy Center (SEC), a thermal power plant situated approximately 19 km southeast of Orlando, Florida, in the United States (Figure 1). The Stanton Energy Center has been actively generating electricity since July 1987, primarily through its thermal power facility known as Stanton 1. To enhance energy production, Stanton 2 was added in 1996. Both power facilities rely on coal as their primary fuel source, with Stanton 1 having a capacity of 444 MW and Stanton 2 with a capacity of 446 MW.

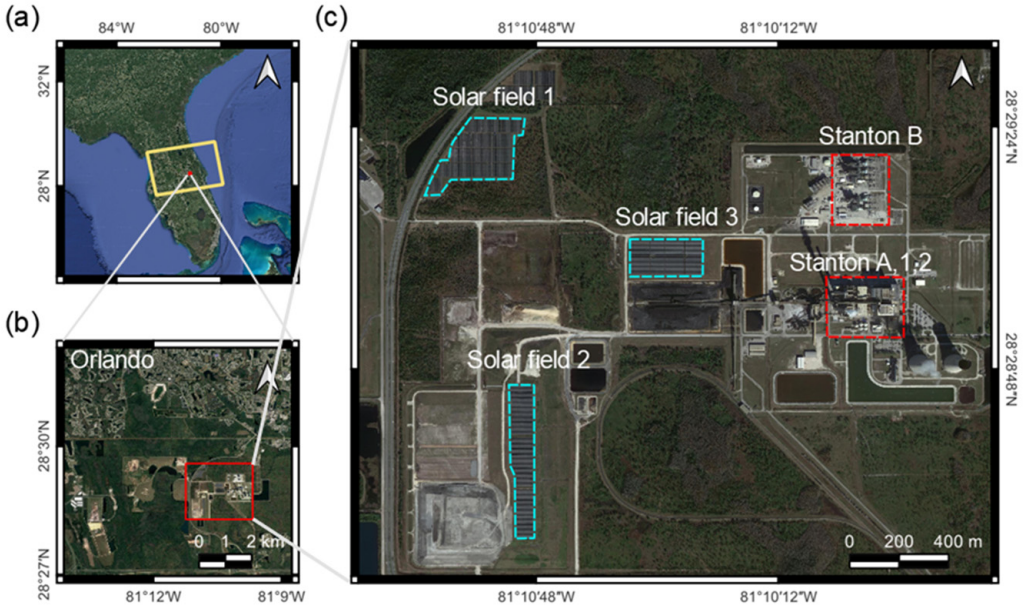

Figure 1. The study area near Stanton Energy Center, Orlando, FL, USA: (**a**) the location of study area with a Sentinel-1 SAR IW image area in a yellow box overlying Google Earth image, (**b**) Orlando region where PSInSAR is applied; and (**c**) Stanton Energy Center with power plants and solar fields in dotted boxes.

Additionally, within the Stanton Energy Center, there is the Stanton A power plant, which utilizes natural gas as its energy source and has been operational since October 2003 with a capacity of 633 MW. Another natural gas-powered plant, Stanton B, has been in operation since February 2010 and has a capacity of 295 MW [27,28]. Moreover, the Stanton Energy Center incorporates solar power as part of its energy generation, with a capacity of 19 MW, contributing to a diverse mix of energy sources at the facility.

Energy production from coal at SEC results in the generation of coal ash, which is managed as industrial waste. To handle this, SEC constructed a landfill situated southwest of the power plant to contain the coal ash contamination. However, as part of their environmental strategy, SEC plans to phase out coal-based electricity generation by the year 2027. Instead, they intend to increase the share of power generation from natural gas-fired plants and solar energy sources [29,30].

Figure 1c shows the installation of solar panels in various areas around the power plant. Specifically, solar fields are present in the northwestern area (Solar Field 1), southwestern area (Solar Field 2), and western area (Solar Field 3). Notably, Solar Field 2 is situated on

top of a coal ash dump, which has been constructed to a height of approximately 25 m. This showcases an innovative approach of repurposing the coal ash dump for clean energy generation using solar panels.

2.2. Dataset

In this research, the PSInSAR analysis utilized Sentinel-1 SAR data provided by the European Space Agency (ESA). Sentinel-1 SAR operates at a C-band frequency with a center frequency of 5.405 GHz and a repeat cycle of 6 days when two satellites (Sentinel-1A and Sentinel-1B) are used [31]. A total of 157 single look complex (SLC) images acquired from the ascending orbit in interferometric wide-swath (IW) mode were used in this study. The incidence angle of the study area is approximately 38.93°, and the nominal resolution is 2.7 m to 3.5 m in the slant range direction and 22 m in the azimuth direction. These images covered the time span from 13 May 2017 to 25 December 2022, and were downloaded from Alaska SAR Facility [32] in path 48 and frame 87. However, it is worth noting that there were limited data available from the descending orbit for PSInSAR analysis. Among the total 156 pairs of DInSAR images used, we had two pairs with a 6-day interval, 141 pairs with a 12-day interval, 24 pairs with a 24-day interval, and one pair with a 36-day interval.

For the DInSAR and PSInSAR analysis in this study, three digital elevation models (DEMs) were considered: shuttle radar topography mission (SRTM) DEM, the Copernicus 30 m DEM, and the LiDAR DEM.

The SRTM DEM was obtained using the space shuttle Endeavor equipped with a C-band radar interferometer [33]. The data collection period for the SRTM DEM was from 11 to 23 February 2000, providing elevation information with a spatial resolution of 30 m [34]. Among the various versions of the SRTM DEM provided by the United States Geological Survey (USGS), SRTM 1Sec HGT was used in this study.

The Copernicus DEM used in this research was derived from data acquired between 29 August 2011 and 22 August 2014 using the bistatic mode of TanDEM-X and TerraSAR-X satellites [35]. It is provided by OpenTopography and CREODIAS and has a spatial resolution of 30 m.

For LiDAR data, the USGS has obtained comprehensive coverage for most areas of the USA, offering LiDAR DEMs with various spatial resolutions [36]. The LiDAR DEM used in this study represents the elevation of the ground surface while eliminating the height of vegetation. Specifically, the study utilized the FL Peninsular FDEM 2018 D19 DRRA 1 m, which was acquired between 4 December 2018, and 12 April 2019, with a spatial resolution of 1 m. These DEMs were critical in the precise analysis of ground subsidence and provided valuable data for the PSInSAR study.

3. Methods

3.1. PSInSAR

The PSInSAR technique involves selecting a master image from a set of (N + 1) SLC images and creating N interferograms by stacking them. By analyzing the spatiotemporal characteristics of the phase of PSs, PSInSAR allows for the measurement of surface displacement over time. PSs are stable scattering points that consistently reflect signals, encompassing artificial structures such as buildings and bridges, as well as natural rocky terrain with high coherence. PSInSAR relies on statistical processing of the temporal phase to distinguish errors from signals and requires a minimum of 20 or more images for accurate results [37–39]. Having more images available enhances the accuracy of the measurements, although it necessitates selecting surface targets with robust temporal stability to be considered as PSs.

In this study, the data processing involved generating 156 DInSAR images using the SNAP (SeNtinel Application Platform) program provided by ESA [40]. The master image, selected from the time series, was from 3 April 2020. For terrain information, the LiDAR DEM was utilized due to its high resolution and recent publicly available data. The PSInSAR data processing was conducted using the Stanford Method for Persistent

Scatterers (StaMPS) program [41]. The perpendicular baseline of the used images ranged up to 228 m, while the temporal baseline spanned from −1056 days to 996 days (see Figure 2). Table 1 presents the major parameters used in the StaMPS data processing, adjusted from the default values to focus on slow ground displacement phenomena such as landslides [42].

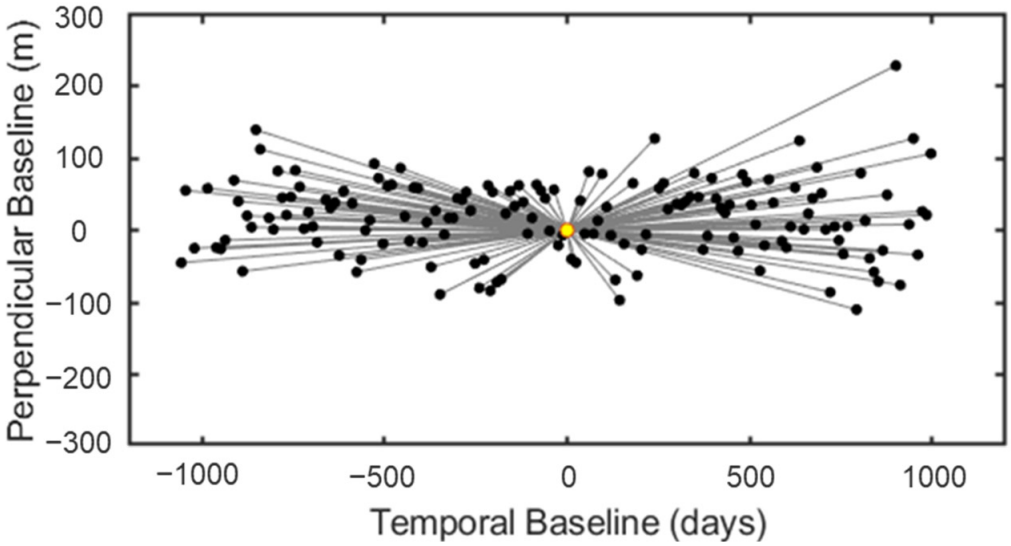

Figure 2. Temporal and perpendicular baseline scatter plot of Sentinel-1 SAR images relative to the master image obtained on 3 April 2020.

Table 1. Several important parameters used in StaMPS Processing.

Parameter	Used
scla_deramp	'y'
scn_time_win	50
unwrap_time_win	24
unwrap_grid_size	10
unwrap_gold_n_win	8

3.2. Ground Range Shift of PS Due to DEM Error

The positions of PS obtained through the PSInSAR technique are geometrically corrected using a DEM. If there are errors in the DEM, however, it can introduce errors in the position of the PS points [43]. Therefore, it is crucial to use a recent DEM that contains height information of the existing structures measured around the same or similar time. For instance, the study area is a landfill site that has been active since the 1990s and is still ongoing as of 2023. Among the areas in the landfill, the section where solar panels were installed was completed in April 2017 after the landfilling. If the SRTM DEM obtained in February 2000 or the Copernicus DEM obtained before 2015 were used for the geometric correction of those solar panel and landfill sites, it can result in inaccurate height information leading to errors in PS point selection. Therefore, it is important to use accurate DEM.

The assessment of positioning errors during the PSInSAR process can be conducted using information provided in Figure 3. The ground range error (δR_g) resulting from the elevation error (Δh) of the DEM is given as follows:

$$\delta R_g = \Delta h \cot \theta_i, \quad (1)$$

where θ_i is the local incidence angle over the surface of the ellipsoidal earth. In this research, three sets of PSInSAR results were obtained using different DEMs: SRTM DEM, Copernicus DEM, and LiDAR DEM. These results were then compared with the height error derived from the LiDAR DEM. The main objective of this comparison was to assess the impact

of DEM errors on the PSInSAR outcomes, helping to understand how variations in the DEM data may affect the accuracy and reliability of the PSInSAR analysis. By conducting this evaluation, the study aims to gain insights into the significance of using precise and up-to-date DEMs in PSInSAR processing and its influence on the final results.

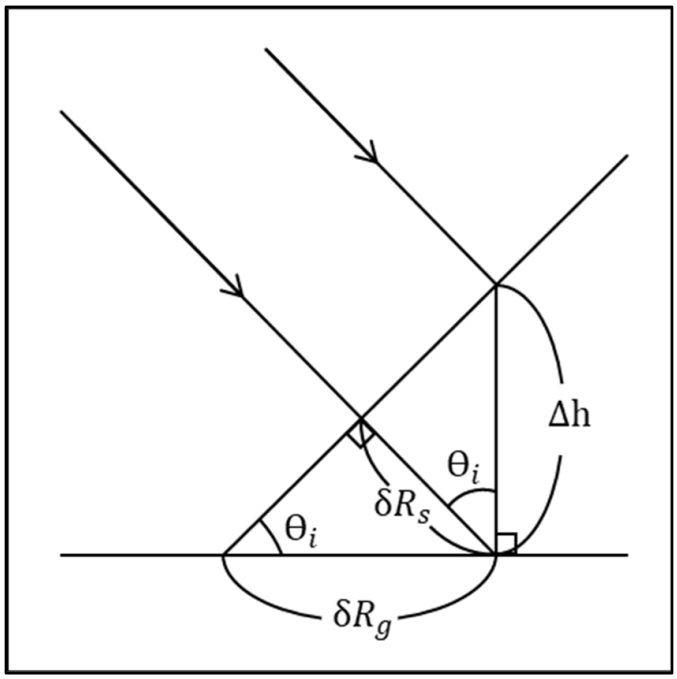

Figure 3. Relation between elevation error (Δh) and ground range error (δR_g). Here, θ_i is incidence angle and δR_s is slant range error.

4. Results

4.1. Temporal Changes in the Landfill Site Using Google Earth Images

Figure 4 illustrates the evolution of the landfill site observed through Google Earth images from 1995 to 2021. In Figure 4a, the image from February 1995 shows the landfill site prepared and ready for deposition. Figure 4b, imaged in February 1999, confirms the initiation of a square-shaped landfill formation in the southern part. As seen in Figure 4c, obtained in March 2006, the landfill slope in the southern part has formed, and the landfill site has expanded towards the north. In the subsequent years, as depicted in Figure 4d–f, the landfill site's elevation gradually increases in the north direction, with images from the years 2008, 2013, and 2016, respectively. Moreover, Figure 4g–i shows that in the years 2017, 2019, and 2021, a new landfill site is being created in the southwestern part of the existing landfill site. Overall, these series of images offer a visual representation of the progressive changes and expansion of the landfill site over the span of more than two decades.

Based on the information provided, the solar field areas for power generation are identified as Solar Field 1, Solar Field 2, and Solar Field 3, based on the completion time of their installation. Solar Field 1 can be observed in the January 2013 image (Figure 4e), while Solar Field 2 is visible in the May 2017 image (Figure 4g). Figure 4g also indicates that approximately half of the panels for Solar Field 3 have been installed, and Figure 4h (November 2019) shows the completion of Solar Field 3. Therefore, it is estimated that the actual completion time for Solar Field 3 is around 2017.

Considering this timeline, it is expected that the solar panels in all three solar fields will exhibit stable scattering characteristics and offer sufficient PS for analysis when applying the PSInSAR technique to the Sentinel-1 SAR data acquired from May 2017 to December 2022. The presence of stable PS points allows for a more robust and reliable PSInSAR analysis to monitor ground displacement and changes over time in these solar field areas.

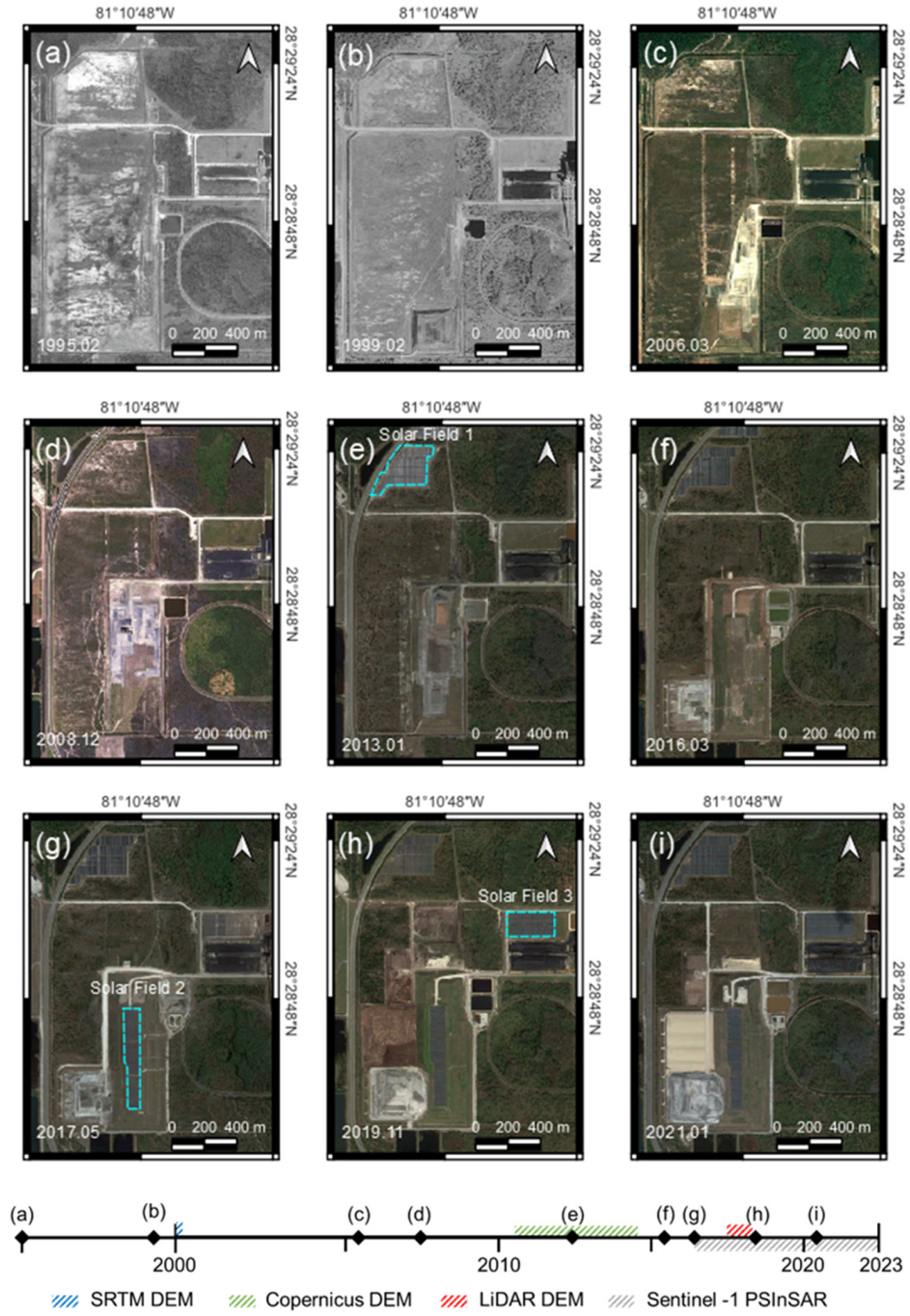

Figure 4. Timeline of Google Earth images of the study area with year and month in YYYY.MM format: (**a**) 1995.02, (**b**) 1999.02, (**c**) 2006.03, (**d**) 2008.12, (**e**) 2013.01, (**f**) 2016.03, (**g**) 2017.05, (**h**) 2019.11, and (**i**) 2021.01.

4.2. Ground Subsidence of Solar Power Plants Using PSInSAR

In Figure 5, the PSInSAR results obtained from processing 157 Sentinel-1 images captured between May 2017 and December 2022, utilizing LiDAR DEM, are overlaid on Google Earth images. The reference area used for the phase unwrapping during the PSInSAR processing was the average value of the entire area, assuming high ground stability in the urban region. The PSInSAR analysis yielded a total of 13,255 PS points, primarily concentrated in the residential areas situated near the southeast of Orlando city. The majority of regions exhibit line of sight (LOS) velocities of approximately 0 mm/yr, depicted by white dots, indicating stable ground conditions in these areas.

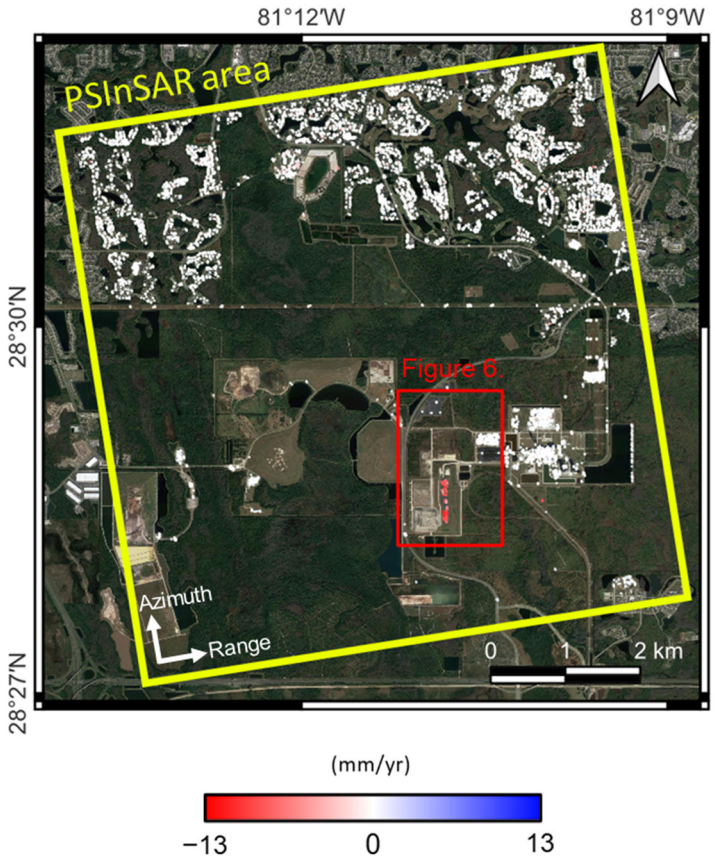

Figure 5. The LOS deformation rate of the study area from PSInSAR.

However, there is a notable localized concentration of PS points showing subsidence velocities in the range of approximately 5–9 mm/yr, represented by the red color in the LOS direction. This subsidence phenomenon is observed in the vicinity of the landfill site for coal ash, situated in the southeastern area near the thermal power plant. The presence of these subsidence areas highlights the significance of monitoring and managing ground stability in proximity to the landfill site to mitigate potential risks associated with subsidence effects.

Figure 6 provides an enlarged view of the area surrounding the landfill site of the thermal power plant, focusing on the temporal ground subsidence phenomena of representative PS points within the solar field. These PS points are indicated in green, and their time-series deformation plots are shown in Figure 6b–d.

For Solar Field 1, it was confirmed that the solar panels were installed on flat ground before 2013. The LOS velocity for a representative PS point within this field was approximately 0.2 mm/yr, indicating a stable ground area within the range of PSInSAR error (Figure 6b). The sparse distribution of PS in Solar Field 1 is due to the rotating solar panels to track the sun. In contrast, for a representative PS point within Solar Field 2, which is installed on top of the landfill site composed of coal ash, the LOS velocity was 5–9 mm/yr, confirming significant subsidence of the ground (Figure 6c). As for Solar Field 3, which is installed on flat ground, the LOS velocity for a representative PS point was approximately 0.6 mm/yr, indicating another stable area within the range of PSInSAR error (Figure 6d).

In conclusion, Solar Field 1 and Solar Field 3 are areas where solar panels are installed on flat ground, and the PSInSAR results indicate stable ground conditions in these regions. No significant structural deformation is observed in the solar panels in these areas. However, Solar Field 2, situated on top of the landfill site composed of coal ash, shows continuous ground subsidence. Despite the ground subsidence, the solar panels themselves exhibit a highly stable structure, suggesting that the observed subsidence in

Solar Field 2 is likely caused by the compression and settling of the coal ash landfill beneath the solar panels.

In the next step, the study aims to further investigate the variations in ground subsidence within Solar Field 2 to gain a better understanding of the specific patterns and mechanisms of subsidence in that area.

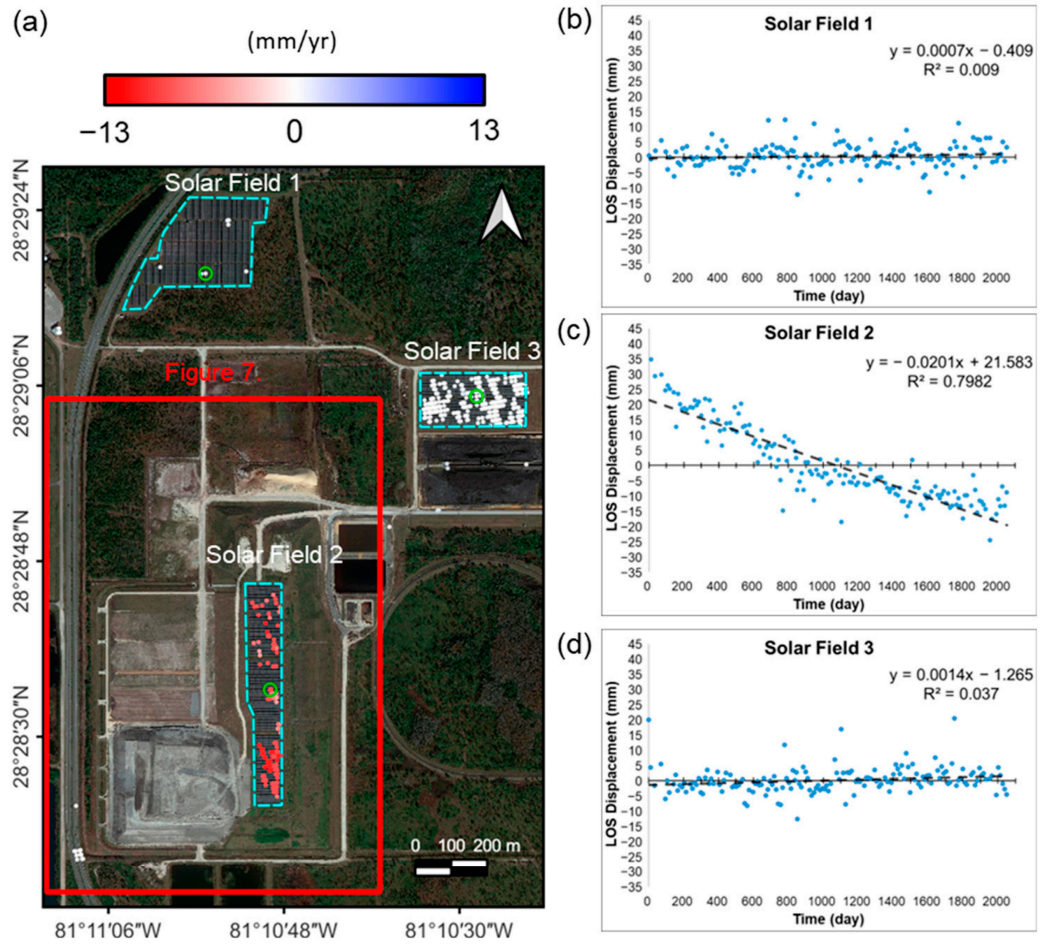

Figure 6. PSInSAR result of solar fields. (**a**) An enlarged image from Figure 5 with green encircled points for representative PS time series LOS deformation of (**b**) Solar Field 1, (**c**) Solar Field 2, and (**d**) Solar Field 3.

4.3. Analysis of Ground Subsidence in the Coal Ash Landfill (Solar Field 2) by Averaging PSInSAR

Based on the analysis using LiDAR DEM and Google Earth images, the upper portion of the coal ash landfill has been categorized into three distinct areas based on the dumping sequence. These areas are designated as Site A, Site B, and Site C, as indicated in Figure 7. Temporal Google Earth images in Figure 4 revealed that the southernmost area, Site C, started receiving coal ash dumping before the year 1999. On the other hand, Site A and Site B continued to receive coal ash until 2016. Afterward, solar panels were installed in these areas before May 2017, marking the transition from landfilling to the installation of the solar field.

These classifications and observations provide valuable insights into the historical sequence of coal ash deposition in different sections of the landfill site, helping to understand the potential variations in ground stability and subsidence patterns in relation to the dumping history and subsequent installation of solar panels.

In Figure 7a, a slight variation in the ground subsidence rate in the LOS direction, obtained from PSInSAR, is depicted for sites A, B, and C. To further analyze the PSInSAR results for each area, Figure 7b–d presents an examination of ground subsidence patterns

by averaging the PS points located above the solar panels within each site. The analysis involved using data from 27, 22, and 70 PS points for Site A, Site B, and Site C, respectively. To ensure the reliability of the results, points with a standard deviation greater than 6 mm and displacements from the LOS direction to the regression line exceeding 10 mm were considered outliers and excluded from the analysis, as shown by the red dots.

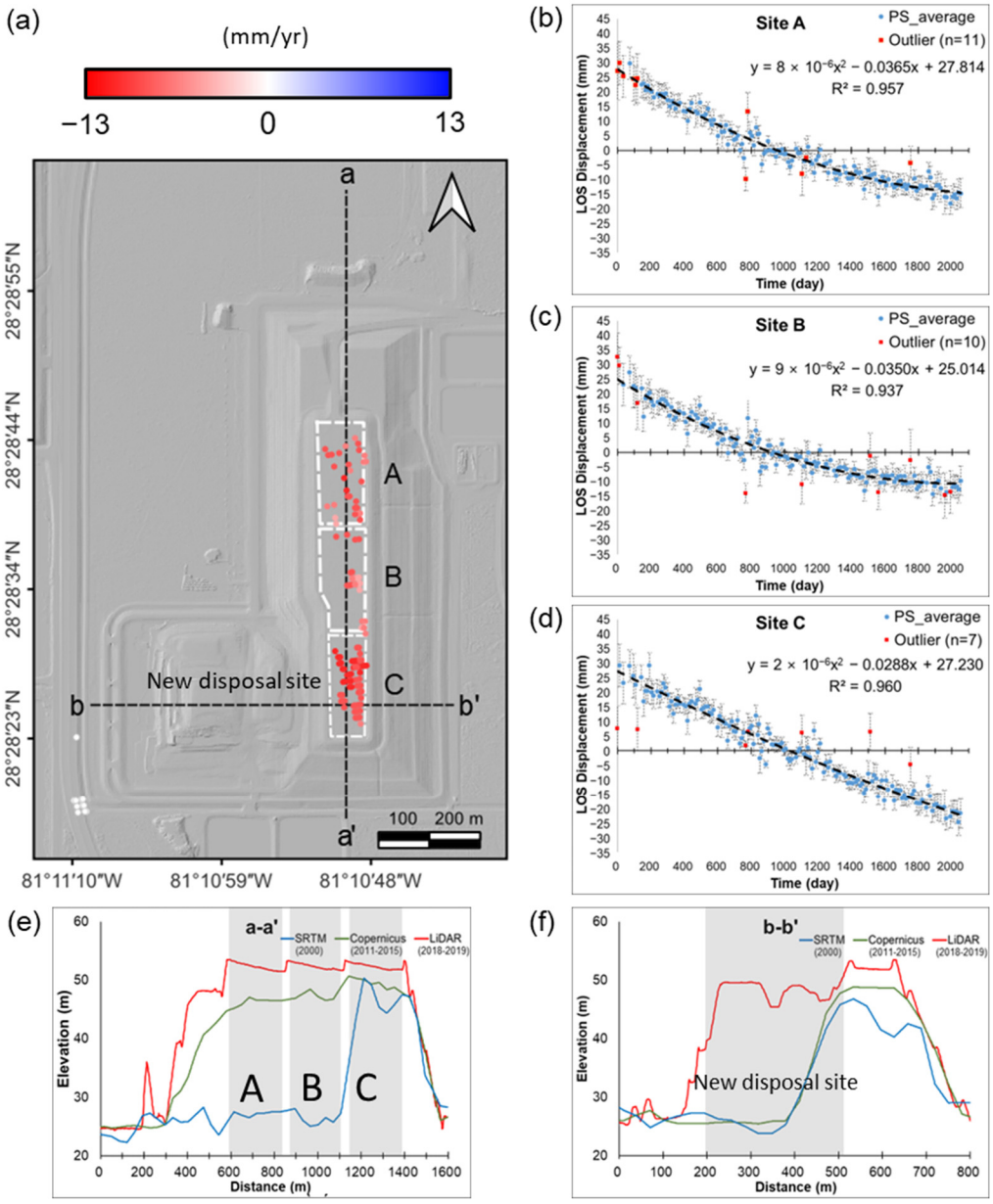

Figure 7. PSInSAR result of solar field 2. (**a**) An enlarged image of Figure 6 with time series averaged plots of (**b**) Site A, (**c**) Site B, and (**d**) Site C. Cross section of DEMs (**e**) along a-a′ and (**f**) along b-b′.

For Site A, the regression equation for the ground subsidence pattern was determined as $y = 8 \times 10^{-6}x^2 - 0.0365x + 27.814$, where x represents the time in days, and y is the LOS displacement in millimeters. The average subsidence rate for Site A was approximately 7.3 mm/yr. As for Site B, its regression equation was found to be $y = 9 \times 10^{-6}x^2 - 0.0350x + 25.014$, resulting in an average subsidence rate of around 6.0 mm/yr. Lastly, for Site C, the regression equation was determined as $y = 2 \times 10^{-6}x^2 - 0.0288x + 27.230$, and the average subsidence rate was approximately 9.0 mm/yr.

Over the course of 5 years and 8 months, sites A, B, and C exhibited subsidence of 41 mm, 33 mm, and 51 mm, respectively. The variation in average subsidence rates

among these sites can be attributed to several factors, including the level of compaction, the composition of the coal ash, and the presence of a cover during the deposition process at each site. These factors may have influenced the stability and settling of the ground in different ways.

In Figure 7a,f, a newly deposited site where coal ash is being added adjacent to Site C can be identified (also seen in Figure 8a). Considering this, it is reasonable to expect that the subsidence rate of Site C, which now bears an additional load from the newly deposited site, would be relatively faster compared to Site A and Site B. However, despite these observations, the study did not find conclusive evidence to pinpoint the exact cause of the differing subsidence rates observed in Sites A, Site B, and Site C. The subsidence process is likely influenced by a combination of complex and site-specific factors, making it challenging to determine a single dominant cause for the observed variations.

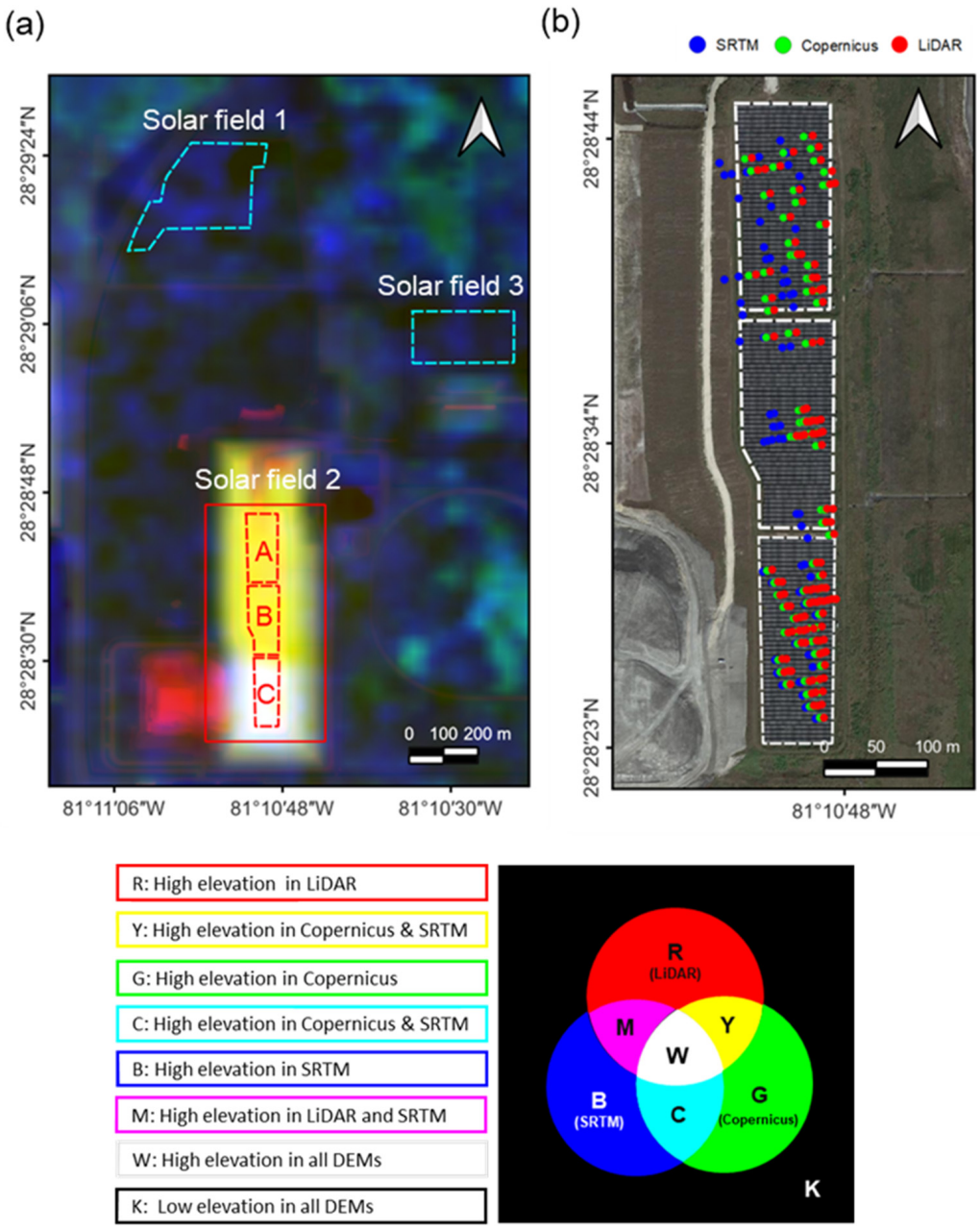

Figure 8. The geometric effect of DEM error on PSInSAR. (**a**) RGB composition of LiDAR (2018–2019), Copernicus (2011–2015), and SRTM (2000) DEMs, respectively. (**b**) PS map using three different DEMs.

The analysis of the quadratic term in the regression equation for the subsidence patterns in sites A, B, and C reveals interesting trends. For Site A and Site B, the quadratic terms are 8×10^{-6} and 9×10^{-6} (mm/day/day), respectively, indicating a parabolic trend where the subsidence rates gradually slow down over time. This suggests that these sites experienced initial rapid subsidence, which then gradually stabilized. In contrast, Site C exhibits a relatively constant subsidence rate, with a quadratic term at 1/4 level (2×10^{-6}) of those observed in Site A and Site B. This means that Site C has maintained a more consistent subsidence rate over time without significant slowing down.

The DEM profile in Figure 7e–f provides further insights. Site C has had a relatively high elevation since the early 2000s, and the additional height of coal ash deposited has remained relatively small, i.e., less than 5 m up until the present. In comparison, sites A and B reached heights of approximately 30 m by around 2012.

Based on these observations, it can be concluded that Site C, which has the longest history of coal ash deposition (over 20 years), exhibited a relatively constant subsidence rate without further slowing down. The constant subsidence rate indicates that the ground stabilization process has reached a more linear trend. Sites A and B, which are more recently deposited and reached significant heights by around 2012, show evidence of initial rapid subsidence during the first 3–5 years, followed by a gradual stabilization with a linear subsidence trend.

In conclusion, the subsidence in the coal ash disposal site seems to follow a general pattern of initial rapid subsidence, which later stabilizes and adopts a more linear subsidence trend over time. The varying rates of subsidence observed in different sites can be attributed to the differences in the duration of deposition, the amount of coal ash accumulated, and the ground stabilization stage in each area.

4.4. Analysis of PS Geometric Errors Due to DEM Errors

In this study, the availability of a relatively high-resolution LiDAR DEM after the construction of dump sites allowed for its application in PSInSAR analysis. When dealing with areas where significant changes in elevation occur, using an appropriate DEM becomes crucial to ensure accurate results. To assess the influence of DEM errors on the geometric correction errors of PSInSAR techniques, we compared the performance of two other DEMs, namely, the SRTM DEM (2000) and the Copernicus DEM (2011–2015), with the most accurate LiDAR DEM (2018–2019). Each DEM was used to obtain PSInSAR results with similar numbers of PS points. However, we observed that the positions of these points were shifted in the range direction when using different DEMs.

To evaluate the reliability of these PS points and their geometric errors, we selected those points for which we could measure the distances between them using different DEMs. These distances were then compared with the geometric errors obtained from the height difference, calculated using Equation (1), considering a representative incidence angle (θ_i) of 38.93°.

Figure 8a provides RGB images of the LiDAR DEM (2018–2019), Copernicus DEM (2011–2015), and SRTM DEM (2000) for the study area. In the landfill area, Site C is depicted as a white color in all three DEMs, indicating a higher elevation compared to the surrounding areas. This suggests that Site C has experienced significant coal ash deposition over the years, leading to an elevated surface. Sites A and B are represented by a yellow color, suggesting that they were relatively flat in the year 2000 (SRTM DEM). However, the elevation of these sites increased after 2015, as seen in the Copernicus DEM and the most recent LiDAR DEM from 2019. This change in elevation indicates that Site A and B received additional coal ash deposition during the period between 2000 and 2019. The red areas on the west of Site C were initially flat until 2015, as shown in the Copernicus DEM. However, the most recent LiDAR DEM from 2019 displays higher elevation values in these areas, indicating new dumping activity that resulted in an increase in ground elevation. In the SRTM DEM, blue areas are observed, indicating higher elevation followed by a decrease in

elevation afterward. These fluctuations in elevation are likely considered as DEM errors, as the SRTM DEM may not accurately capture the terrain variations in this region.

First, the measured horizontal distance differences and the distances calculated based on the elevation differences for sites A, B, and C were found to be well matched with the overall RSME of 1.21 m (Figure 9). The error is within the expected range during DEM resampling or distance measurement. This suggests that by utilizing the elevation differences from the DEM, it is possible to determine the appropriate distribution of PS in the landfill area and correct the position information of the PS in the time series. Subsequently, the maximum, minimum, and average distances were compared for each site in Tables 2 and 3.

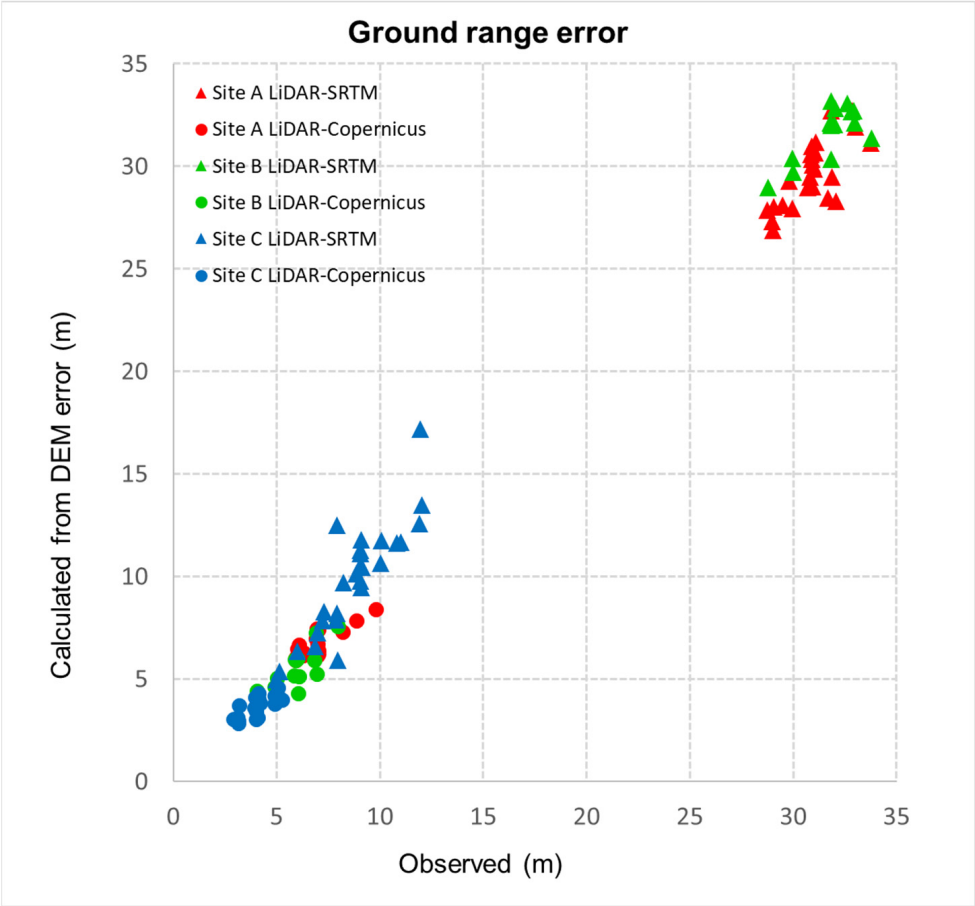

Figure 9. Comparison of the observed and calculated ground range error due to DEM error.

Table 2. Statistics on the observed and calculated ground range error due to the deviation of the Copernicus DEM from LiDAR DEM.

Ground Range Error (m)	Min	Max	Average	RMSE
Site A observed	5.93	9.78	6.84	0.58
Site A calculated	5.91	8.39	6.61	
Site B observed	4.06	7.95	6.05	0.78
Site B calculated	4.30	7.69	5.75	
Site C observed	2.90	5.27	4.20	0.66
Site C calculated	2.85	4.57	3.75	

When comparing the PSInSAR results using Copernicus and LiDAR for the landfill site (Table 2), Site A had a total of 24 PS points. The measured horizontal distance differences ranged from a minimum of 5.93 m to a maximum of 9.78 m, with an average of 6.84 m. The

calculated horizontal distance differences ranged from 5.91 m to 8.39 m, with an average of 6.61 m. In Site B, using a total of 15 PS points, the obtained horizontal distances were from 4.06 m to 7.95 m, with an average of 6.05 m, which matched with the calculated horizontal distances from 4.30 m to 7.69 m, with an average of 5.75 m. In Site C, with a total of 27 PS points, the obtained horizontal distance differences were from 2.85 m to 4.57 m, with an average of 3.75 m. The calculated horizontal distance differences were from 2.90 m to 5.27 m, with an average of 4.20 m.

Table 3. Statistics on the observed and calculated ground range error due to the deviation of the SRTM DEM from LiDAR DEM.

Ground Range Error (m)	Min	Max	Average	RMSE
Site A observed	28.73	33.75	30.89	1.66
Site A calculated	26.86	32.73	29.60	
Site B observed	28.79	33.79	31.80	0.89
Site B calculated	28.98	33.19	31.71	
Site C observed	4.98	12.03	8.69	1.79
Site C calculated	4.98	17.20	9.80	

Table 3 shows the comparison of the PSInSAR results using the SRTM DEM and LiDAR DEM. For Site A, the measured horizontal distance differences ranged from 28.73 m to 33.75 m, with an average of 30.89 m. The calculated horizontal distance differences ranged from 26.86 m to 32.73 m with an average of 29.60 m. In Site B, the measured horizontal distances were from 28.79 m to 33.79 m, with an average of 31.80 m, while the calculated horizontal distances were from 28.61 m to 33.19 m, with an average of 31.80 m. For Site C, the measured horizontal distance differences were from 4.98 m to 12.03 m, with an average of 8.69 m, while the calculated horizontal distance differences were from 4.98 m to 17.20 m, with an average of 9.80 m.

Sites A and B experienced an elevation increase of approximately 25 m between the acquisition of SRTM (2000) and Copernicus (2011–2015) DEM data due to the dumping of coal ash. On the contrary, the elevation increase between the acquisition of Copernicus and LiDAR (2018–2019) DEM data was less than 8 m, mostly due to the installation of the solar panels. The overall elevation increase in Site C was much smaller when compared to sites A and B. Therefore, the difference between the measured and the calculated horizontal distances obtained from site C are smaller when compared to sites A and B.

In summary, the differences in elevation changes and ground positioning error patterns at Site A, Site B, and Site C between different DEM acquisitions provide valuable insights into the geologic and anthropogenic factors influencing ground stability and subsidence in the landfill area. These findings help to improve the understanding of the PSInSAR results and enhance the accuracy of ground subsidence monitoring and analysis in the study area.

5. Discussion

In this study, the PSInSAR method was used to measure surface displacement in coal ash landfills and solar panel installation areas using Sentinel-1 SAR data and LiDAR DEM. The PSInSAR results provided the displacement of each PS in the LOS direction, which is specific to the ascending orbit only. Unfortunately, there were limited data available from the descending orbit for the study area, which prevented the calculation of displacement components in the east–west and up–down directions. As a result, it was not possible to conclusively determine if the displacement of the landfill site was purely vertical subsidence or if it also contained any horizontal motion. Ideally, data collection from both ascending and descending orbits is recommended for PSInSAR studies, as it allows for a more comprehensive understanding of ground displacement in multiple directions.

Based on the LOS displacement measured by PSInSAR and considering the incidence angle of 38.93° in the study area, it was estimated that the vertical subsidence of sites A, B,

and C are approximately 53 mm, 42 mm, and 66 mm, respectively, over the entire image acquisition period of 5 years and 8 months. These estimates assume that the subsidence in the coal ash sites is purely gravitational and occurs only in the vertical direction. However, it is essential to interpret these results with caution, as the lack of data from the descending orbit may introduce uncertainties in the vertical displacement estimates. Additional data from both orbits would be required to obtain a more complete understanding of the ground subsidence and to analyze the displacement in multiple directions accurately.

Spatial averaging of the PSInSAR time series deformation data used in Section 4.3 is a valuable approach that allows us to group together PS points with similar characteristics, such as being made of the same material (e.g., solar panels) and being part of the same underlying landfill site. This assumption is reasonable as it helps to simplify the analysis and provides a more coherent representation of the ground subsidence patterns within each averaging group. By applying spatial averaging, we can effectively reduce the noise in the data and improve the accuracy of the results.

PS points within each averaging group are expected to exhibit similar radar signals and stable behavior over the study period, which justifies the coherence observed among them. Furthermore, the identification and removal of outliers based on higher standard deviation and large deviations from the quadratic regression function are essential steps in ensuring the reliability of the analysis. Outliers can introduce noise and inaccuracies into the results, and by removing them, we can focus on the more consistent and representative PS points within each averaging group. Overall, the spatial averaging technique and the removal of outliers contribute to producing more robust and meaningful results, enabling a better understanding of the ground subsidence phenomena associated with the solar panel installation and the landfill site.

The reference level in dealing with various DEMs, such as the SRTM DEM and Copernicus DEM using the earth ellipsoid as a reference and the LiDAR DEM using the geoid, can introduce discrepancies in the altitude values. The 29 m offset in the altitude value in the Orlando, Florida area must be taken into account to ensure accurate comparisons and interpretations. Additionally, when using different DEMs for PSInSAR analysis, there can be difficulties in matching PSs between the results obtained with these DEMs. PS points might not perfectly correspond one-to-one, and their patterns and distributions could vary. As a result, selecting a limited number of PSs that appear to be a pair or exhibit similar patterns becomes necessary to mitigate the potential geometric errors during the analysis. It is essential to acknowledge these challenges and uncertainties when working with multiple DEMs and PSInSAR data, as they can affect the accuracy and reliability of the results. Properly accounting for reference level discrepancies and selecting suitable PSs for analysis are critical steps in addressing these issues and obtaining meaningful insights from the PSInSAR study.

6. Conclusions

In this study, ground subsidence at Stanton Energy Center, located in Orlando, Florida, were analyzed by applying the PSInSAR technique to a total of 157 Sentinel-1 SAR images obtained from May 2017 to December 2022. In addition, the development process of the coal ash landfill sites and the construction of solar panels within the research area was identified over time using decadal Google Earth images. Within the research area, three solar panel zones were present, and it was observed that the area where solar panels were installed on the landfill site (Solar Field 2) showed a subsidence of 5–9 mm/year in the LOS direction. However, stable PSInSAR results were observed in the remaining flat areas where solar panels were installed (Solar Field 1 and 3), indicating that the subsidence was not caused by structural issues with the solar panels themselves, but rather by the coal ash landfill site subsiding.

To analyze the landfill site in more detail, Solar Field 2 was divided into three areas: Site A, Site B, and Site C. The overall ground subsidence patterns in each site were analyzed by spatially averaging the PSInSAR results. The subsidence velocities in Site A, Site B, and

Site C were determined to be 7.3 mm/year, 6.2 mm/year, and 8.8 mm/year, respectively, indicating ground subsidence in those areas. Assuming vertical subsidence only, they correspond to 53 mm, 42 mm, and 66 mm vertical subsidence for 5 years and 8 months.

The time-series deformation of Site A and Site B showed a quadratic curve in time, while that of Site C appeared linear. The difference in subsidence trend is possibly due to recent dumping of the coal ash in Site A and Site B less than 10 years ago, where the subsidence rate is fast at first and then slows down over time. On the other hand, Site C is considered to have completed dumping more than 20 years ago and shows that the ground subsiding proceeds at a constant rate.

The study also compared the geometric error of PS points resulting from elevation differences between different DEMs (SRTM DEM, Copernicus DEM, and LiDAR DEM). The use of recent and accurate DEMs is crucial, especially when dealing with varying terrain.

Continuous monitoring of ground subsidence in landfill sites using PSInSAR, with readily available SAR data such as Sentinel-1 SAR or future data from NISAR (NASA-ISRO), is recommended for more comprehensive and precise assessments. This monitoring approach can provide valuable insights into the long-term behavior of landfill sites and assist in environmental management and planning.

Author Contributions: Conceptualization, Y.S. and H.L.; methodology, Y.S. and H.L.; software, Y.S.; validation, Y.S.; formal analysis, Y.S. and H.L.; investigation, Y.S.; resources, H.L.; data curation, Y.S.; writing—original draft preparation, Y.S.; writing—review and editing, H.L.; visualization, Y.S.; supervision, H.L.; project administration, H.L.; funding acquisition, H.L. All authors have read and agreed to the published version of the manuscript.

Funding: This research was supported by the National Research Foundation of Korea, grant no. NRF-2022R1F1A1071054 and no. 2019R1A6A1A03033167, and by the Ministry of the Interior and Safety as Human Resource Development Project in Disaster Management.

Data Availability Statement: The data presented in this study are available on request from the corresponding author.

Conflicts of Interest: The authors declare no conflict of interest. The funders had no role in the design of the study; in the collection, analyses, or interpretation of data; in the writing of the manuscript; or in the decision to publish the results.

References

1. British Petroleum. Available online: https://www.bp.com/content/dam/bp/business-sites/en/global/corporate/pdfs/energy-economics/statistical-review/bp-stats-review-2021-full-report.pdf (accessed on 26 May 2023).
2. Heidrich, C.; Feuerborn, H.; Weir, A. Coal Combustion Products: A Global Perspective. *VGB Power Tech.* **2013**, *93*, 46–52.
3. Ferreira, C.; Ribeiro, A.; Ottosen, L. Possible Applications for Municipal Solid Waste Fly Ash. *J. Hazard. Mater.* **2003**, *96*, 201–216. [CrossRef]
4. Al Biajawi, M.I.; Embong, R.; Muthusamy, K.; Ismail, N.; Obianyo, I.I. Recycled Coal Bottom Ash as Sustainable Materials for Cement Replacement in Cementitious Composites: A Review. *Constr. Build. Mater.* **2022**, *338*, 127624. [CrossRef]
5. Ahmaruzzaman, M. A Review on the Utilization of Fly Ash. *Prog. Energy Combust. Sci.* **2010**, *36*, 327–363. [CrossRef]
6. Pandey, V.C.; Singh, N. Impact of Fly Ash Incorporation in Soil Systems. *Agric. Ecosyst. Environ.* **2010**, *136*, 16–27. [CrossRef]
7. Kravchenko, J.; Lyerly, H.K. The Impact of Coal-Powered Electrical Plants and Coal Ash Impoundments on the Health of Residential Communities. *N. Carol. Med. J.* **2018**, *79*, 289–300. [CrossRef] [PubMed]
8. Yoo, H.K.; Choi, B.H. Analysis of factors affecting the slope stability of uncontrolled waste landfill. *J. Korean Geo-Environ. Soc.* **2002**, *3*, 5–12.
9. Cowan, E.A.; Seramur, K.C.; Hageman, S.J. Magnetic Susceptibility Measurements to Detect Coal Fly Ash from the Kingston Tennessee Spill in Watts Bar Reservoir. *Environ. Pollut.* **2013**, *174*, 179–188. [CrossRef]
10. Ruhl, L.; Vengosh, A.; Dwyer, G.S.; Hsu-Kim, H.; Deonarine, A.; Bergin, M.; Kravchenko, J. Survey of the Potential Environmental and Health Impacts in the Immediate Aftermath of the Coal Ash Spill in Kingston, Tennessee. *Environ. Sci. Technol.* **2009**, *43*, 6326–6333. [CrossRef]
11. Ramsey, A.B.; Faiia, A.M.; Szynkiewicz, A. Eight Years After the Coal Ash spill–Fate of Trace Metals in the Contaminated River Sediments Near Kingston, Eastern Tennessee. *Appl. Geochem.* **2019**, *104*, 158–167. [CrossRef]
12. Lemly, A.D. Damage Cost of the Dan River Coal Ash Spill. *Environ. Pollut.* **2015**, *197*, 55–61. [CrossRef] [PubMed]

13. Yang, Y.; Colman, B.P.; Bernhardt, E.S.; Hochella, M.F. Importance of a Nanoscience Approach in the Understanding of Major Aqueous Contamination Scenarios: Case Study from a Recent Coal Ash Spill. *Environ. Sci. Technol.* **2015**, *49*, 3375–3382. [CrossRef] [PubMed]
14. Deonarine, A.; Bartov, G.; Johnson, T.M.; Ruhl, L.; Vengosh, A.; Hsu-Kim, H. Environmental Impacts of the Tennessee Valley Authority Kingston Coal Ash Spill. 2. Effect of Coal Ash on Methylmercury in Historically Contaminated River Sediments. *Environ. Sci. Technol.* **2013**, *47*, 2100–2108. [CrossRef]
15. Bartov, G.; Deonarine, A.; Johnson, T.M.; Ruhl, L.; Vengosh, A.; Hsu-Kim, H. Environmental Impacts of the Tennessee Valley Authority Kingston Coal Ash Spill. 1. Source Apportionment using Mercury Stable Isotopes. *Environ. Sci. Technol.* **2013**, *47*, 2092–2099. [CrossRef]
16. Ferretti, A.; Monti-Guarnieri, A.; Prati, C.; Rocca, F.; Massonet, D. *InSAR Principles-Guidelines for SAR Interferometry Processing and Interpretation*; ESA Publication: Noordwijk, The Netherlands, 2007.
17. Pepe, A.; Calò, F. A Review of Interferometric Synthetic Aperture RADAR (InSAR) Multi-Track Approaches for the Retrieval of Earth's Surface Displacements. *Appl. Sci.* **2017**, *7*, 1264. [CrossRef]
18. Han, H.; Lee, H. Surface Strain Rates and Crevassing of Campbell Glacier Tongue in East Antarctica Analysed by Tide-Corrected DInSAR. *Remote Sens. Lett.* **2017**, *8*, 330–339. [CrossRef]
19. Ferretti, A.; Prati, C.; Rocca, F. Nonlinear Subsidence Rate Estimation using Permanent Scatterers in Differential SAR Interferometry. *IEEE Trans. Geosci. Remote Sens.* **2000**, *38*, 2202–2212. [CrossRef]
20. Ferretti, A.; Prati, C.; Rocca, F. Permanent Scatterers in SAR Interferometry. *IEEE Trans. Geosci. Remote Sens.* **2001**, *39*, 8–20. [CrossRef]
21. Peltier, A.; Bianchi, M.; Kaminski, E.; Komorowski, J.; Rucci, A.; Staudacher, T. PSInSAR as a New Tool to Monitor Pre-eruptive Volcano Ground Deformation: Validation using GPS Measurements on Piton De La Fournaise. *Geophys. Res. Lett.* **2010**, *37*, L12301. [CrossRef]
22. Kothyari, G.C.; Joshi, N.; Taloor, A.K.; Malik, K.; Dumka, R.; Sati, S.P.; Sundriyal, Y.P. Reconstruction of Active Surface Deformation in the Rishi Ganga Basin, Central Himalaya using PSInSAR: A Feedback Towards Understanding the 7th February 2021 Flash Flood. *Adv. Space Res.* **2022**, *69*, 1894–1914. [CrossRef]
23. Oliveira, S.C.; Zêzere, J.L.; Catalão, J.; Nico, G. The Contribution of PSInSAR Interferometry to Landslide Hazard in Weak Rock-Dominated Areas. *Landslides* **2015**, *12*, 703–719. [CrossRef]
24. Pawluszek-Filipiak, K.; Borkowski, A. Monitoring Mining-Induced Subsidence by Integrating Differential Radar Interferometry and Persistent Scatterer Techniques. *Eur. J. Remote Sens.* **2021**, *54*, 18–30. [CrossRef]
25. Lee, H.; Moon, J.; Lee, H. Activity of Okgye Limestone Mine in South Korea Observed by InSAR Coherence and PSInSAR Techniques. *Remote Sens.* **2022**, *14*, 6261. [CrossRef]
26. Choi, E.; Moon, J.; Kang, T.; Lee, H. Observation of Volume Change and Subsidence at a Coal Waste Dump in Jangseong-dong, Taebaek-si, Gangwon-do by Using Digital Elevation Models and PSInSAR Technique. *Korean J. Remote Sens.* **2022**, *38*, 1371–1383. (In Korean) [CrossRef]
27. Orlando Utilities Commission. Fuel Diversity. 2022. Available online: https://www.ouc.com/environment-community/green-initiatives/stanton-energy-center/fuel-diversity (accessed on 19 May 2023).
28. Curtis, H. Stanton Energy Center. 2023. Available online: https://floridadep.gov/water/siting-coordination-office/content/curtis-h-stanton-energy-center (accessed on 26 May 2023).
29. Orlando Utilities Commission. 2020 Electric Integrated Resource Plan Report. pp. 1–2. Available online: https://oucroadmap.com/executive-summary-siemens-report (accessed on 19 May 2023).
30. Williams, J.H.; Jones, R.A.; Torn, M.S. Observations on the Transition to a Net-Zero Energy System in the United States. *Energy Clim. Chang.* **2021**, *2*, 100050. [CrossRef]
31. ESA Sentinel-1. Available online: https://sentinels.copernicus.eu/web/sentinel/missions/sentinel-1/overview (accessed on 19 May 2023).
32. Alaska Satellite Facility. Available online: https://search.asf.alaska.edu/#/ (accessed on 19 May 2023).
33. USGS SRTM. Available online: https://www.usgs.gov/centers/eros/science/usgs-eros-archive-digital-elevation-shuttle-radar-topography-mission-srtm-1 (accessed on 19 May 2023).
34. Hanssen, R.F. *Radar Interferometry: Data Interpretation and Error Analysis*; Springer Science & Business Media: Berlin, Germany, 2001.
35. ESA Copernicus DEM. Available online: https://spacedata.copernicus.eu/collections/copernicus-digital-elevation-model (accessed on 19 May 2023).
36. USGS LiDAR Data Download. Available online: https://apps.nationalmap.gov/lidar-explorer/#/ (accessed on 19 May 2023).
37. Crosetto, M.; Monserrat, O.; Cuevas-González, M.; Devanthéry, N.; Crippa, B. Persistent Scatterer Interferometry: A Review. *ISPRS J. Photogramm. Remote Sens.* **2016**, *115*, 78–89. [CrossRef]
38. Hooper, A.; Segall, P.; Zebker, H. Persistent Scatterer Interferometric Synthetic Aperture Radar for Crustal Deformation Analysis, with Application to Volcán Alcedo, Galápagos. *J. Geophys. Res. Solid Earth* **2007**, *112*. [CrossRef]
39. Hooper, A. A Multi-temporal InSAR Method Incorporating both Persistent Scatterer and Small Baseline Approaches. *Geophys. Res. Lett.* **2008**, *35*. [CrossRef]
40. SNAP Download. Available online: https://step.esa.int/main/download/snap-download/ (accessed on 19 May 2023).

41. StaMPS. Available online: https://homepages.see.leeds.ac.uk/~earahoo/stamps/ (accessed on 19 May 2023).
42. Höser, T. Analysing the Capabilities and Limitations of InSAR Using Sentinel-1 Data for Landslide Detection and Monitoring. Master's Thesis, University of Bonn, Bonn, Germany, 2018.
43. Jung, J.; Kim, D.; Palanisamy Vadivel, S.K.; Yun, S. Long-Term Deflection Monitoring for Bridges using X and C-Band Time-Series SAR Interferometry. *Remote Sens.* **2019**, *11*, 1258. [CrossRef]